

## ***Predicting GaN Device Lifetimes In Solar Microinverters And Power Optimizers***

*by Shengke Zhang, Siddhesh Gajare and Ricardo Garcia, Efficient Power Conversion, El Segundo, Calif.*

Microinverters and power optimizers are widely utilized in modern solar panels to maximize energy efficiency and conversion. Such topologies and implementations usually require a minimum of 25 years of lifetime, which is becoming a critical challenge for market adoption. Low-voltage gallium nitride (GaN) power devices ( $V_{DS}$  rating < 200 V) are a promising solution and are being used extensively by an increasing number of solar manufacturers.

In this article, a test-to-fail approach is adopted and applied to investigate the intrinsic underlying wear-out mechanisms of GaN transistors. The study enables the development of physics-based lifetime models that can accurately project the lifetimes under the unique demands of various mission profiles in solar applications.

After reviewing the benefits that are driving the switch from string inverters to microinverters and power optimizers in photovoltaic systems, the test-to-fail methodology is introduced and the three device “stressors” most likely responsible for device failure are identified—gate bias, drain bias and temperature cycling. In the subsequent sections, the impact of each of these factors on device lifetime, expressed in terms of mean time to failure (MTTF) and other parameters, is assessed.

As we’ll see, one of the three stressors dominates in determining device reliability and the influence of this factor will be analyzed here in greater depth. The physical causes of device failure under the dominant stressor are explained and a mathematical model is presented that can be used to predict GaN device lifetime. Use of the model is illustrated with a real-world example.

### ***Trends In Photovoltaic Power Conversion***

The ever-increasing demand for renewable energy sources has led to a rapid growth in rooftop solar installations across residential and commercial sectors. Traditionally, string inverters have been widely employed in solar installations, where multiple solar panels are connected in series. The inverter is responsible for converting direct current (dc) output from solar panels to alternating current (ac) electricity that can be used to power homes.

String inverters have served as a reliable choice for years. However, they also face many challenges, including reduced performance due to shading, panel mismatch issues, and a lack of module-level monitoring. Most importantly, due to the series configuration of the string inverters, the lowest performing panel dominates the energy conversion rate of the entire system, which could significantly lower the system efficiency.

The Department of Energy released the \$1/watt photovoltaic (PV) system initiative in 2010, where developing higher efficiency and more reliable module-level integrated inverters was highlighted as the key area of improvement to meet the target.<sup>[1]</sup> The SunShot 2030 PV program envisions a similar cost target by 2030.<sup>[2]</sup> To meet the goals and maximize energy production, emerging technologies such as microinverters and power optimizers have gained significant attention.

Microinverters are small, individual inverters that are attached to each solar panel, allowing for dc to ac power conversion at the panel level. This enables each solar panel to function at its peak performance by using independent maximum power point tracking (MPPT). Even if a tree branch shades certain panels, all the neighboring panels can still convert at their full capacity. The drop in efficiency only affects the panels in the shade.

Independent tracking also allows solar users to monitor the health of each panel easily. If a panel requires repair, it won’t bring down the whole system. In addition, microinverters make it easy to add panels to increase power output. Microinverters can be more expensive than string inverters but can pay off over time by getting more power from your system. Therefore, microinverters in the market need to match panel guarantees with 25-year warranties.<sup>[3,4]</sup>

Power optimizers are dc-dc converters integrated into the solar panel wiring, enabling MPPT of each individual solar panel by continually regulating the dc characteristics to maximize energy output. A power optimizer is a good solution for situations where shading is an issue, or the panels must be placed on multiple roof surfaces with different orientations. Therefore, power optimizers generally are a more energy efficient solution than string inverters. The power optimizer also requires 25 years of warranty.<sup>[5,6]</sup>

### Test-To-Fail Methodology

To address the reliability concerns surrounding the requirement for 25 years of reliable operation, a test-to-fail approach<sup>[7,8]</sup> is adopted and applied to GaN devices that are commonly used in solar applications. The methodology involves stressing the devices under test (DUTs) to cause them to fail quickly under accelerated conditions while monitoring type and time of failure.

By analyzing the failures and understanding the underlying failure mechanisms, physics-based lifetime models can be developed to explain the unique characteristics of GaN. The developed models can be used to accurately project the lifetimes under all mission profiles that are unique to solar applications.

By examining the mission profiles for solar applications, three key reliability stressors are identified; gate bias, drain bias and temperature cycling (TC).

When multiple failure mechanisms or stressors are involved, the total failure rate, commonly denoted as failure in time (FIT), is the sum of the failure rates per failure mechanism<sup>[9,10]</sup> as shown below,

$$FIT_{Total} = FIT_1 + FIT_2 + \dots + FIT_i \quad (1)$$

where an FIT represents the number of failures per  $10^9$  (billion) device hours, and the subscript indicates the different failure mechanisms identified.

FIT is inversely proportional to mean time to failure (MTTF) as described by references 9 and 10,

$$FIT = 10^9 / MTTF \quad (2)$$

Therefore, by plugging equation (2) into equation (1), the total MTTF can be described by equation (3),

$$\frac{1}{MTTF_{Total}} = \frac{1}{MTTF_{Gate}} + \frac{1}{MTTF_{Drain}} + \frac{1}{MTTF_{TC}} \quad (3)$$

where the different failure mechanisms (1, 2, 3... i) are replaced with the three reliability stressors that are relevant to solar applications, as discussed above. Based on equation (3), it is noted that the smallest denominator or the stressor that yields the least MTTF dominates the overall lifetime of the devices.

Therefore, it is critical to understand which stressor is the limiting factor in reliability. This stressor warrants more consideration during design and operation.

In this article, each stressor is studied independently by using this test-to-fail approach, where the individual intrinsic wear-out mechanism is successfully identified, and the corresponding lifetime is determined.

### Gate Bias

GaN high electron mobility transistors (HEMTs) are used in dc-ac (microinverters) or dc-dc (power optimizers) topologies in their solar applications. The gate terminal must be biased periodically during switching. Hence, gate reliability over time is the first stressor to examine.

Four groups of representative GaN HEMTs (EPC2212) and 32 devices per group were tested under four different accelerated stress conditions, where the bias voltages of 8 V, 8.5 V, 9 V, and 9.5 V well exceeded the max rated gate voltage ( $V_{GS(max)}$ ) of 6 V. At 9 V and 9.5 V, failures occurred very quickly, but it took significantly longer at 8 V and 8.5 V. The test-to-fail data involving gate reliability for representative GaN

HEMTs was presented in reference 7. After the failures were identified, failure analyses were conducted on a large number of failures at all test voltages, and a consistent failure mode was found.

Fig. 1 shows the failure mode observed in all failures analyzed. The location of the gate failures is where the silicon nitride dielectric is sandwiched between gate metal and field plate metal.

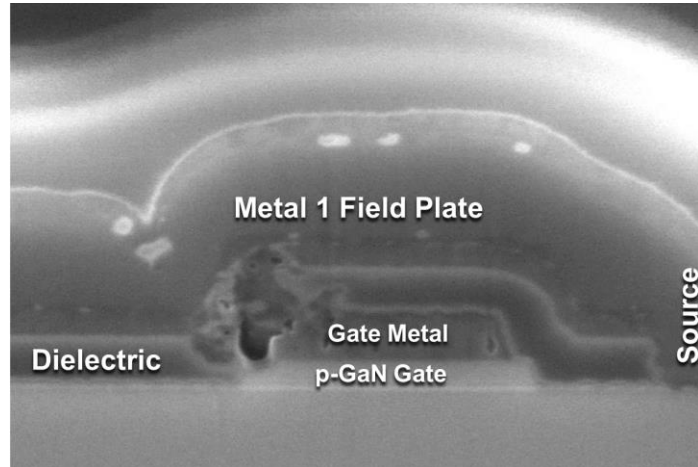


Fig. 1. Scanning electron microscopy (SEM) image of a gate failure. Dielectric breakdown is observed between the gate metal and the field plate metal.

To explain all the observations found via failure analysis, an impact ionization model was introduced and developed in a two-step process.<sup>[7]</sup> In the first step, electrons within the two-dimensional electron gas (2DEG) enter the p-GaN gate and get accelerated under the influence of positive gate bias within gate. In this process some electrons gain sufficient energy to cause impact ionization and generate holes.

In the second step, the generated holes near the top surface of the gate move away from the gate corner to the field plate metal (source potential) under the positive electric field due to the positive gate bias. As a result, the holes become trapped in the silicon nitride dielectric layer, leading to a growing positive charge density. When the trapped charges accumulate and reach the critical field of the silicon nitride dielectric film, it ruptures catastrophically, leading to the failure shown in Fig. 1.

Impact ionization is a well-known phenomenon in GaN devices.<sup>[11-14]</sup> Equation (4) is the final expression that derives from the impact ionization physical process as given in reference 7.

$$MTTF(V_{GS}, \Delta T) = \frac{A}{(1-c\Delta T)} \exp \left[ \left( \frac{B}{V_{GS} + V_0} \right)^m \right] \quad (4)$$

where  $V_{GS}$  is the gate bias and  $\Delta T$  is the temperature relative to 25°C;  $m = 1.9$ ,  $V_0 = 1.0$  V,  $B = 57$  V,  $A = 1.7 \times 10^{-6}$  seconds, and  $c = 6.5 \times 10^{-3} \text{ K}^{-1}$ .

Equation (4) is plotted against recently measured data for the EPC2212 in Fig. 2. As shown in the figure, GaN HEMTs have an approximately 1-ppm failure rate projected after 25 years of continuous dc bias at  $V_{GS(\max)} = 6$  V. The projected lifetime results are also consistent with EPC's field experience, where no gate failures have been identified in 13 years of shipment.

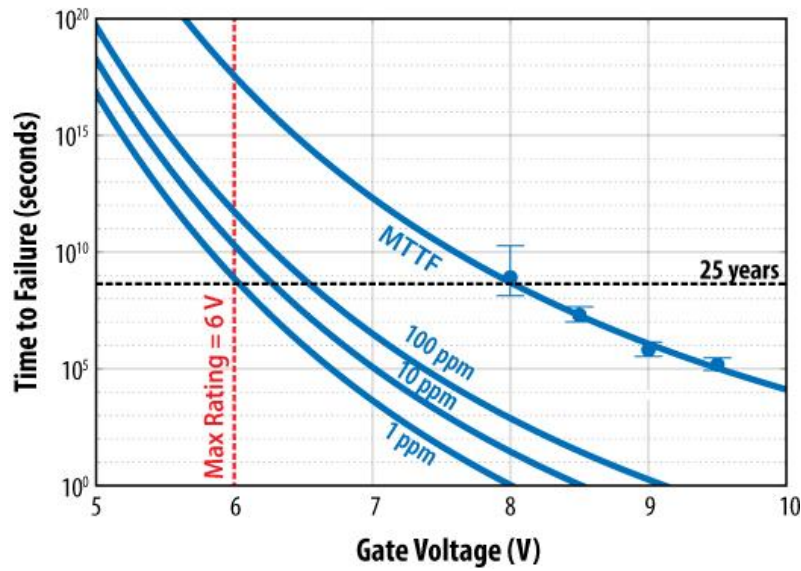


Fig. 2. Time to failure vs. gate bias at 25°C. MTTF (and error bars) are shown for four different voltage legs. The solid line corresponds to the impact ionization lifetime model equation (4) at different failure rates, including MTTF (63.2%), 100 ppm, 10 ppm, and 1 ppm.

## Drain Bias

The low on-resistance ( $R_{DS(ON)}$ ) and small die size of GaN HEMTs significantly increase the power conversion efficiency and reduce the power losses in microinverter and dc-dc converter applications. However, one common concern for GaN is dynamic on-resistance. This is a condition whereby the  $R_{DS(ON)}$  of GaN HEMTs increases when the device is exposed to high drain-source voltage ( $V_{DS}$ ). The dominant wear-out mechanism responsible for the rise in  $R_{DS(ON)}$  is electron trapping near the channel.<sup>[7,8]</sup> As the trapped charges accumulate, electrons are depleted from the finite pool available in the 2DEG during the on state, leading to an increase in  $R_{DS(ON)}$ .

A resistive hard-switching topology circuit with in-situ  $R_{DS(ON)}$  monitoring and active temperature control was developed and implemented to accelerate the electron trapping effect by providing significantly more trapping candidates at and beyond the max rated  $V_{DS}$ . By conducting extensive testing, a first-principles lifetime model was developed to describe this electron trapping process and how it can be correlated with the dynamic  $R_{DS(ON)}$  test results. The final expression is shown in equation (5),<sup>[7,8]</sup>

$$\frac{\Delta R}{R} = a + b \log\left(1 + \exp\left(\frac{V_{DS} - V_{FD}}{\alpha}\right)\right) \sqrt{T} \exp\left(\frac{\hbar\omega_{LO}}{kT}\right) \log(t) \quad (5)$$

where  $V_{DS}$  = drain voltage (V),  $T$  = device junction temperature (K),  $t$  = time (min);  $a = 0$  (unitless),  $b = 2 \times 10^{-5} \text{ (K}^{-1/2}\text{)}$ ,  $\hbar\omega_0 = 92 \text{ meV}$ ,  $\alpha = 10 \text{ V}$ , and  $V_{FD}$  varies with the device  $V_{DS}$  rating (for example,  $V_{FD} = 100 \text{ V}$  for the 100-V devices discussed in this work).

The flyback is one of the more popular topologies for microinverters in solar applications. When selecting the appropriate GaN transistors for the primary side, three main contributing factors to the drain voltage are considered. These are (1) the bus voltage, (2) the flyback voltage, and (3) the voltage overshoot due to ringing caused by the parasitic inductance in the design.

The typical bus voltage for a microinverter is 60 V in a solar application. The flyback voltage is determined by the product of the system's output voltage and the turns ratio of the transformer. By adding some margin for the voltage overshoot and derating, a 170-V maximum  $V_{DS}$  rating is frequently desired by the solar customers using such topology.

The EPC2059<sup>[15]</sup> is a 170-V maximum  $V_{DS}$  rated product that meets the general requirements for microinverters in solar applications. Fig. 3 shows the in-situ  $R_{DS(on)}$  test results of a representative EPC2059 device that was operated under continuous hard switching at 136 V (80% of the max rated drain bias of 170 V) while the case temperature was modulated at 80°C. This temperature is used because it is considered the nominal operating temperature for solar panels.

As shown in Fig. 3, the lifetime model of equation (5) is plotted against the measured data. The model predicts the  $R_{DS(on)}$  increase due to continuous hard switching in 25 years to be approximately 10%.

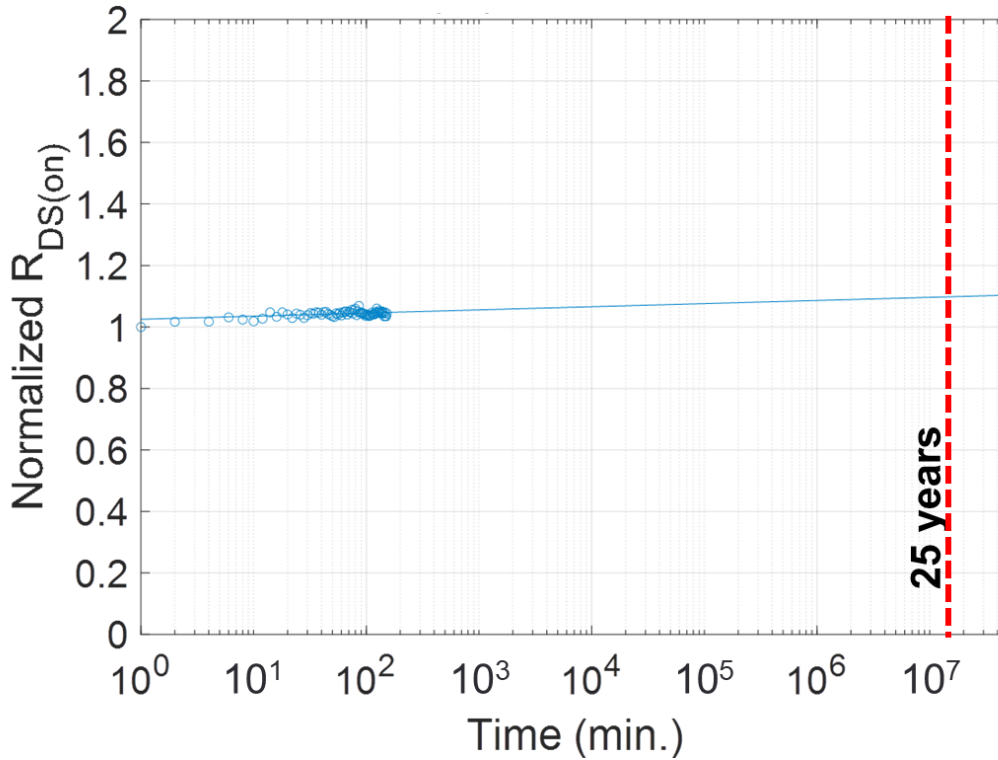


Fig. 3. The projected  $R_{DS(on)}$  shift of the EPC2059, a 170-V rated device, in 25 years of 100-kHz continuous hard-switching operation at 136 V is approximately 10%. The blue circles represent measured data.

Another popular option for solar systems is to use a dc-dc converter in a power optimizer. This has been adopted by many solar providers due to its superior efficiency. EPC’s GaN devices such as the 100-V rated EPC2218<sup>[16]</sup> and EPC2302,<sup>[17]</sup> among others, are good fits for this application.

Fig. 4 plots the results obtained with the lifetime model from equation (5) alongside the in-situ measured data for two representative devices—the EPC2218 and EPC2302. A shift of less than 10% in 25 years of continuous hard switching at 80% of the max rated drain bias and 100 kHz is expected.

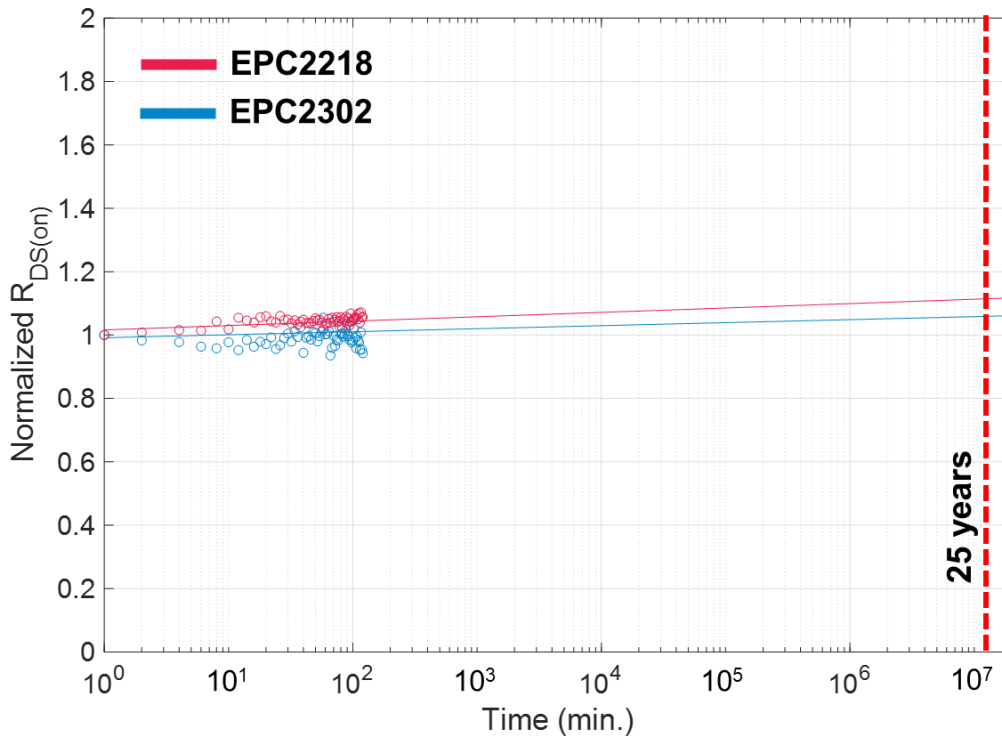


Fig. 4. The projected  $R_{DS(on)}$  shifts of the EPC2218 and the EPC2302, which both are 100-V rated devices, under continuous hard-switching operation at 80 V, 100 kHz are plotted here. The blue and red circles represent measured data.

This result suggests that dynamic  $R_{DS(ON)}$  failure mode is not the dominant limiting factor in equation (3) for EPC’s GaN devices under the mission profiles for solar applications.

### Temperature Cycling

Temperature cycling is another critical area of particular interest for solar applications. Solar panels are placed outside and experience significant ambient temperature change each day. Therefore, devices mounted on the printed circuit boards (PCBs) in the solar panels must be capable of surviving 25 years of continuous ambient temperature change.

A similar test-to-fail approach was applied to study the board-level thermomechanical reliability of the EPC2218A,<sup>[18]</sup> the automotive grade of the EPC2218. As described above, either the automotive-grade EPC2218A, or equivalent commercial-grade 100-V rated devices are ideal candidates for use in power optimizers for solar applications.

Three different combinations of temperature cycling stress conditions, with and without underfill material were studied. Two temperature cycling ranges were tested: temperature cycle 1 (TC1):  $-40^{\circ}\text{C}$  to  $125^{\circ}\text{C}$  and temperature cycle 2 (TC2):  $-40^{\circ}\text{C}$  to  $105^{\circ}\text{C}$ .

Over the temperature range of TC1, two cases were compared—one with, and one without underfill material. The underfill material selected was from Henkels Loctite (part number: Eccobond-UF 1173) which showed good performance in previous studies.<sup>[19]</sup> The detailed selection guideline for identifying proper underfill materials is also discussed in reference 19.

For all cases, the parts were mounted on DUT cards consisting of a two-layer, 1.6-mm thick, FR4 board using SAC305 solder paste, and water-soluble flux. All underfilled devices were subjected to a plasma clean process

prior to the underfill application. Industry standard (JESD22-A108F<sup>[20]</sup>) as well as other customers' specifications were followed for this study.

A group of 88 EPC2218A devices were tested for each test leg, and all three legs used similar ramp rate and dwell time at the two temperature extremes. After every temperature cycling interval, electrical screening was performed. Exceeding datasheet limits was used as the criterion for failure. Physical cross-sectioning and SEM inspection were followed to further examine the electrical test failures. Solder joint cracking was found to be the single failure mode throughout all failures analyzed. The experimental results from the test-to-fail approach are summarized in Weibull plots in Fig. 5.

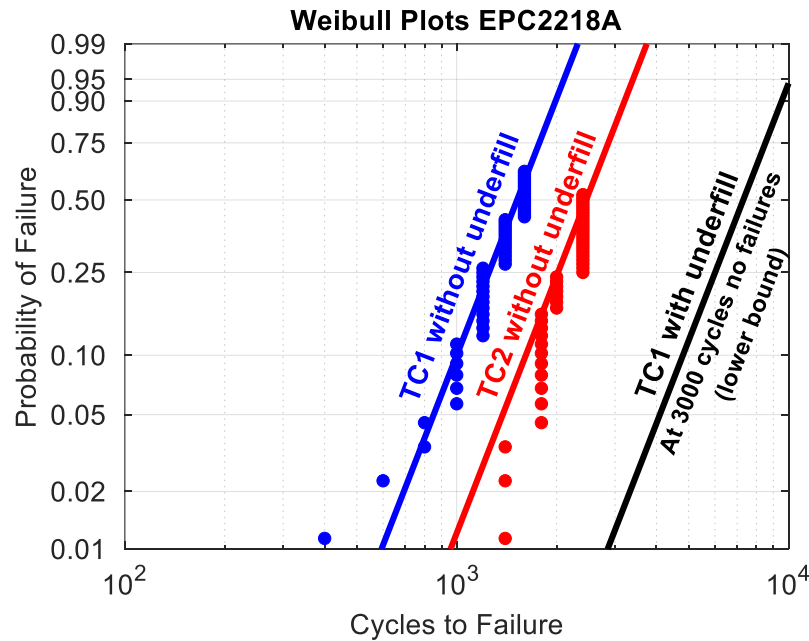


Fig. 5. Weibull plots of temperature cycling results for EPC2218A.

The TC1 (−40°C to 125°C) tests without underfill material reached more than 50% cumulative failures at 1600 cycles, where physical failure analysis found that solder joint cracking was the single failure mode for all failures at various read points. The TC2 (−40°C to 105°C) tests without underfill achieved 50% failure rate after 2400 cycles. The data in Fig. 5 shows that a larger temperature range accelerates the time of failure in TC stress.

Two primary failure mechanisms could be responsible for the acceleration. First, the difference in  $\Delta T$  of two testing conditions leads to the acceleration of the solder fatigue failure mechanism, which is well described by the Coffin-Manson relation and is widely adopted by JEDEC<sup>[21]</sup> and AEC<sup>[22]</sup> standards. However, this failure mechanism alone is insufficient to explain the acceleration observed.

A second mechanism, creep solder joint failure, is introduced. Creep is believed to be the main factor during the dwell period at the hot temperature extremes.<sup>[23-27]</sup> This creep mechanism is governed by an activation energy that will be discussed in the following lifetime model development.

After 3000 cycles of TC1 (−40°C to 125°C) with Henkel underfill, no outlier devices were found in the absolute  $R_{DS(ON)}$  value, nor in  $R_{DS(ON)}$  shift post electrical testing. All parameters examined showed very tight distributions throughout all temperature cycling intervals.

Physical cross-sectioning was conducted randomly on the 3000-cycle passing devices, where no solder joint cracking was observed. This shows that applying proper underfill material can significantly improve the TC capability of the chip-scale package devices. Therefore, the Weibull fit line for the TC1 with the underfill leg is merely the lower bound confidence level based on the current test results. The test is still in progress.

To understand the main failure mechanisms involved in board-level temperature cycling, a more-general lifetime model was developed by using the Norris-Landzberg model.<sup>[23]</sup>

$$N = A \cdot f^{-\alpha} \cdot \Delta T^{-\beta} \cdot \exp\left(\frac{E_a}{kT_{Max}}\right) \quad (6)$$

where  $N$  is the number of cycles to fail,  $f$  is the cycling frequency and  $\alpha$  is the cycling frequency exponent. This frequency term  $f$  is to describe the frequency of usage.

In this study, the cycling frequency is determined by counting the total number of cycles per day and the cycling frequency exponent  $\alpha$  that is widely used is  $-1/3$ .<sup>[24-28]</sup>  $\Delta T$  is the range of temperature change in one cycle and  $\beta$  is the temperature range exponent. This  $\beta$  term is the well-known Coffin-Manson relation mentioned above<sup>[15-16]</sup> and is used to determine the effect of the  $\Delta T$ . The temperature range exponent is typically around 2. Since SAC305 solder is used in this study, the exponent  $\beta$  in this case is 2.3 for the lifetime modeling.<sup>[20-26]</sup>

The last variable is an Arrhenius term that focuses on the creep failure mechanism at the maximum temperature,  $T_{Max}$  in each cycle, where  $E_a$  is the activation energy,  $k$  is the Boltzmann constant, and  $T_{Max}$  is the maximum temperature of the high-temperature dwell stage in Kelvin (K).

Finding the activation energy is critical, and the last step towards developing the lifetime model. By comparing the MTTF between TC1 and TC2 without underfill material as listed in the table, the acceleration factor was determined. Based on this acceleration factor, the activation energy ( $E_a$ ) at  $T_{Max}$  was calculated to be 0.18 eV.

Table. Temperature cycling profile and MTTF determined by Weibull plots.

TC condition	$\Delta T(^{\circ}\text{C})$	Cycle duration (min)	Frequency (cycles per day)	MTTF (cycles)
TC1 without underfill	165	40	36	1505
TC2 without underfill	145	30	48	2430
TC1 with underfill	165	40	36	7230 (lower bound confidence level)

The projected lifetime curves using the Norris-Landzberg model are plotted in Fig. 6 assuming the  $T_{Max}$  is  $125^{\circ}\text{C}$ , which is possibly the worst-case scenario for the creep failure mechanism. The horizontal, black-dashed line at 9,125 cycles represents a duration of 25 years of continuous operation assuming one thermal cycle per day.

Fig. 6 shows that after 25 years of continuous operation under a constant temperature swing of  $72^{\circ}\text{C}$  from hot to cold, or vice versa, only 0.1% of the EPC2218A devices with underfill material would fail the datasheet limit due to an increase in  $R_{DS(ON)}$  value. At a 1% failure rate, 99% of the devices should be capable of surviving 25 years of continuous operation when subjected to a constant  $\Delta T$  of  $95^{\circ}\text{C}$ . Even without underfill material, 99% of the parts should survive a fixed  $\Delta T$  of approximately  $51^{\circ}\text{C}$  over 25 years of lifetime.

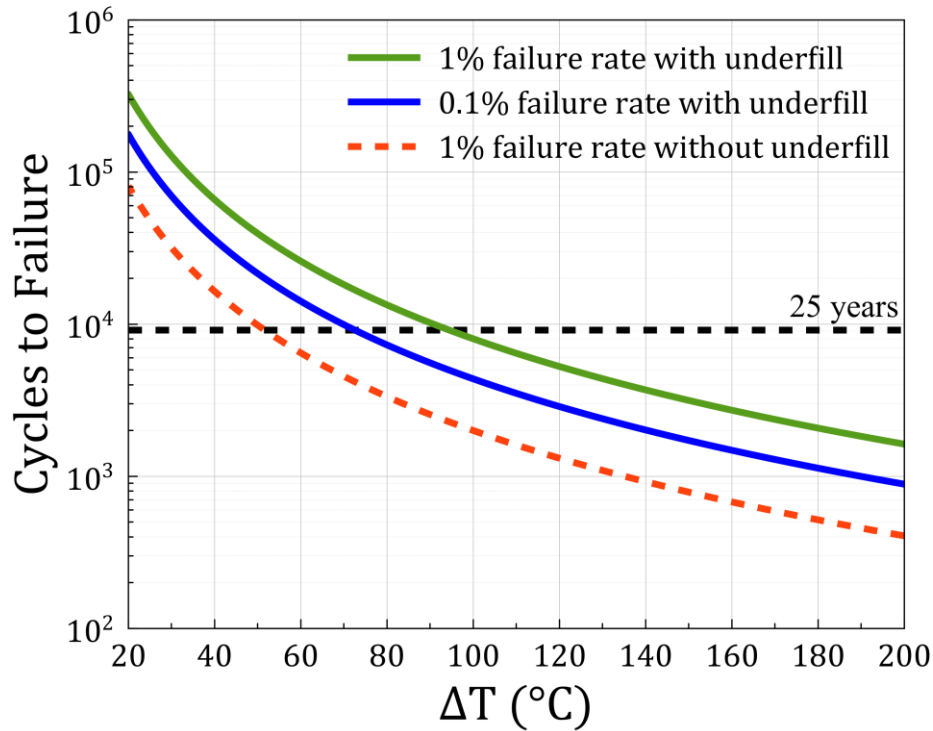


Fig. 6. Lifetime prediction curves for EPC2218A with respect to  $\Delta T$  using the Norris-Landzberg model.

In real world applications, solar panels experience varying ambient temperatures, and the amount of temperature change varies significantly depending on the season and location. As a result, a more-general lifetime model for thermo-mechanical stress is warranted to account for all mission profiles over the 25 years of lifetime. An empirical mathematical model is developed below to account for different  $\Delta T$  at different seasons of the year, as shown in equation (7).

$$\frac{1}{N_{Total}} = \frac{a}{N_{\Delta T_a}} + \frac{b}{N_{\Delta T_b}} + \dots + \frac{i}{N_{\Delta T_i}} \quad (7)$$

where  $N_{Total}$  is the total calculated lifetime number of cycles,  $N_{\Delta T_a}$  corresponds to cycles-to-failure for the condition of  $\Delta T_a$  and  $a$  is the fraction of time the device was operational under the condition of  $\Delta T_a$ ,  $N_{\Delta T_b}$  corresponds to cycles-to-failure for the condition of  $\Delta T_b$  and  $b$  is the fraction of time the device was operational under  $\Delta T_b$ , and  $N_{\Delta T_i}$  corresponds to cycles-to-failure for the condition of  $\Delta T_i$  and  $i$  is the fraction of time the device was operational under  $\Delta T_i$ .

There are three main factors that predominantly determine the lifetime of the solder joints when developing this model. Each one is included in the model.

1. The duration of each mission profile needs to be separated. This effect is accounted for by the fractional coefficient in the numerator of each term in equation (2), such as  $a$ ,  $b$ , ..., and  $i$ .
2. The temperature change ( $\Delta T$ ) in each mission profile. This term is addressed by the Norris-Landzberg model in equation 1 and plotted in Fig. 6. The solder joints experience the most stress during the period when the devices are subjected to the largest  $\Delta T$ , which translates to the shortest cycles-to-failure. The overall lifetime of the device essentially will be dominated by the most stressful period. This effect is addressed by putting the cycles-to-failure terms ( $N_{\Delta T}$ ) in the denominator and then summing them up collectively.
3. The hottest temperature extreme of each cycle, or the baseline temperature. For instance, the solder joints may experience different stress levels given an identical  $\Delta T$  in the winter or in the summer. This effect is

included in the Arrhenius term in equation (6), which eventually goes to the cycles-to-failure term ( $N_{\Delta T}$ ) in the denominators of equation (7).

Now let's examine a real-world example to estimate the lifetime using equation (7) by applying different mission profiles throughout the lifetime of the devices, where the calculation uses the lifetime plot of the 0.1% failure rate for the EPC2218A with underfill.

First, let's assume the solar panels are installed in Phoenix, Arizona, U.S.A., where solar is well-suited for the climate, which has long sun exposure, but also demands very stringent thermo-mechanical requirements due to the extreme temperature changes over time. Use the weather report history of Phoenix, Arizona as an example.<sup>[29]</sup>

In addition, 30°C of device self-heating is added to the ambient temperature change for the total lifetime calculations. For the 0.01% failure rate, or 100 ppm, which means 100 devices failed in 1 million parts tested, the EPC2218A with underfill is projected to have 18,218 cycles to failure, equivalent to 49.9 years of lifetime operation considering one cycle per day for GaN devices in the example application.

If we extrapolate to a 0.001% failure rate, or 10 ppm, suggesting only 10 failures out of 1 million devices tested, now the total lifetime is calculated to be 10,971 cycles. This is equivalent to approximately 30 years of continuous operation with one cycle per day.

The results imply that temperature cycling is the most critical stressor that could be limiting the overall lifetime for GaN used in solar applications. However, by using proper underfill materials TC reliability can be significantly improved to exceed the required 25 years of continuous operation with a low failure rate under nominal solar mission profiles.

## Conclusions

The test-to-fail results and physics-based lifetime projections show that neither gate bias nor drain bias is a reliability concern for microinverters or power optimizers in solar applications. Using appropriate underfill materials can vastly reduce thermal cycling reliability risk while giving excellent lifetimes that significantly exceed the expected 25-year lifetime.

## References

1. "[\\$1/W Photovoltaic Systems: white paper to explore a grand challenge for electricity from solar](#)," U.S Department of Energy, August 2010.
2. "[SunShot 2030 for Photovoltaics \(PV\): Envisioning a Low-cost PV Future](#)" by W. Cole, B. Frew, P. Gagnon, J. Richards, Y. Sun, J. Zuboy, M. Woodhouse, and R. Margolis, National Renewable Energy Laboratory, Golden, CO (2017).
3. "[Enphase IQ 7-Based M-Series Microinverters](#)," Enphase Energy data sheet, February 2023.
4. "[IQ8M and IQ8A Microinverters](#)," Enphase Energy data sheet, April 2023.
5. "[SolarEdge Power Optimizer Module Embedded Solution, OPJ300-LV](#)," SolarEdge data sheet, January 2023.
6. "[Power Optimizer Frame-Mounted P370/P401/P404/P500](#)," SolarEdge data sheet, May 2023.
7. *GaN Power Devices and Applications* by A. Lidow, El Segundo, Calif., PCP Press, 2021.
8. "In-situ RDS(ON) Characterization and Lifetime Projection of GaN HEMTs under Repetitive Overvoltage Switching" by R. Zhang, R. Garcia, R. Strittmatter, Y. Zhang and S. Zhang, IEEE Transactions on Power Electronics, doi: 10.1109/TPEL.2023.3290117.
9. "System Reliability" edited by C. Volosencu, InTechOpen, 2017. doi: 10.5772/66993.

10. "Method for Calculating Failure Rates in Units of FITS," JEDEC Standard JESD85A, January 2014.
11. "Measurement of Impact Ionization Coefficients in GaN" by A.M. Ozbek, Ph.D. thesis, North Carolina State University, 2012.
12. "Mean multiplication gain and excess noise factor of GaN and Al<sub>0.45</sub>Ga<sub>0.55</sub>N avalanche photodiodes" by T.L. Ooi, P. L. Cheang, A.H. You, and Y.K. Chan, European Physical Journal-Applied Physics, 92, 10301. (2020).
13. "Experimental characterization of impact ionization coefficients for electrons and holes in GaN grown on bulk GaN substrates" by L. Cao, J. Wang, G. Harden, H. Ye, R. Stillwell, A. J. Hoffman, and P. Fay, Applied Physics Letters, 112, 262103, 2018.
14. "Experimental determination of impact ionization coefficients of electrons and holes in gallium nitride using homojunction structures" by D. Ji, B. Ercan, and S. Chowdhury, Appl. Phys. Lett. 115, 073503 (2019).
15. "[EPC2059 – Enhancement-mode power transistor](#)," EPC2059 datasheet, Efficient Power Conversion.
16. "[EPC2218 – Enhancement-mode power transistor](#)," EPC2218 datasheet, Efficient Power Conversion.
17. "[EPC2302 – Enhancement-mode power transistor](#)," EPC2302 datasheet, Efficient Power Conversion.
18. "[EPC2218A – Enhancement-mode power transistor](#)," EPC2218A datasheet, Efficient Power Conversion.
19. "EPC GaN transistor application readiness: phase fourteen testing" by A. Pozo, S. Zhang, and R. Strittmatter, Reliability Report, Efficient Power Conversion.
20. "Temperature Cycling," JEDEC Standard, Test Method JESD22-A104F, November 2020.
21. "Stress-Test-Driven Qualification of Integrated Circuits," JEDEC Standard, JESD47L, December 2022.
22. "Failure Mechanism Based Stress Test Qualification For Discrete Semiconductors In Automotive Applications," AEC-Q101-Rev E, Automotive Electronics Council, March 2021.
23. "Reliability of Controlled Collapse Interconnections" by K. C. Norris and A. H. Landzberg, IBM Journal of Research and Development, 13(3), pp. 266–271, 1969.
24. "An Acceleration Model for Lead-Free (SAC) Solder Joint Reliability Under Thermal Cycling" by V. Vasudevan and X. Fan, ECTC 2008, pp. 139–145.
25. "Modified Norris–Landzberg Model and Optimum Design of Temperature Cycling Alt." by F.Q. Sun, J.C. Liu, Z.Q. Cao, X.Y. Li and T.M. Jiang, Strength Mater 48, 135–145 (2016).
26. "Norris–Landzberg Acceleration Factors and Goldmann Constants for SAC305 Lead-Free Electronics" by P. Lall, A. Shirgaokar, and D. Arunachalam, ASME. Journal of Electronic Packaging, 134(3), 031008, 2012.
27. "Fatigue Life of Joint-Scale SAC305 Solder Specimens in Tensile and Tensile and Shear Mode" by A. Deshpande, Q. Jiang, A. Dasgupta, and U. Becker, 2019 18th IEEE Intersociety Conference on Thermal and Thermomechanical Phenomena in Electronic Systems (ITherm), Las Vegas, NV, USA, 2019, pp. 1026-1029.
28. "Accelerated Temperature Cycle Test and Coffin-Manson Model for Electronic Packaging" by H. Cui, RAMS, pp. 556-560, 2005.
29. [MSN weather data for Phoenix, Arizona](#).

## About The Authors



*Shengke Zhang is vice president of reliability at Efficient Power Conversion (EPC) where he leads the product reliability and failure analysis for GaN transistors and ICs. Prior to joining EPC, he worked on RF-MEMS devices in the mobile industry. Shengke is the author or co-author of more than 30 technical papers. He also serves as a committee member for JEDEC's JC-70 Wide Bandgap Power Electronic Conversion Semiconductors Committee. Shengke earned his Ph.D. degree in Materials Science and Engineering from Arizona State University investigating low-loss dielectrics for cellular and quantum computing applications.*



*Siddhesh Gajare is a reliability and failure analysis engineer at EPC, where he is responsible for bringing reliable gallium nitride (GaN) technology to the market. He received his Ph.D. degree in Materials Science and Engineering from Arizona State University investigating the origin of microwave loss in dielectric resonators under the supervision of Nathan Newman.*



*Ricardo Garcia is a senior test engineer at EPC, where he leads GaN IC reliability testing and characterization. Ricardo also has extensive experience in high and low power supplies. Prior to joining EPC, Ricardo worked on the development of the test equipment and procedures to ensure product quality and safety at Ametek Programmable Power. Ricardo received his B.S. degree in electrical engineering from the University of California, San Diego.*

*For more on reliability in power converter design, see How2Power's [Design Guide](#), locate the "Design area" category and select "Reliability". For more on designing with GaN power devices, see the "Popular Topics" category and select "Silicon Carbide and Gallium Nitride".*